Nanoscale Advances

ROYAL SOCIETY OF CHEMISTRY

PAPER

View Article Online
View Journal | View Issue

Cite this: *Nanoscale Adv.*, 2025, **7**, 6248

Report on the relevance of perovskite module outdoor ageing performance and indoor UV degradation trend

Lu Zhang,†[a] Dongxue Liu,†[b] Guiting Du,†[c] Long Cai,[c] Wanlei Dai,[a] Yixin Dong,[b] Huitao Dai,[b] Yongshuai Gong,[b] Shengxiong Zhang,[a] Buyi Yan*[a] and Jizhong Yao*[a]

Perovskite solar cells have made remarkable progress in laboratory-scale efficiency, positioning them as a promising next-generation photovoltaic technology. However, their long-term operational stability under real-world conditions remains a critical barrier to commercial deployment. This study presents a three-year outdoor field investigation of a micro power station composed of 20 perovskite sub-modules ($FA_{0.9}Cs_{0.1}PbI_3$-based, each measuring 30 cm × 40 cm), deployed in subtropical eastern China and fabricated using scalable, industry-compatible processes. The system was continuously monitored over a three-year period to assess its long-term energy output and operational stability under real-world conditions. In parallel, we developed a spectral-accelerated ageing protocol using a tailored ultraviolet to blue-violet light spectrum, with enhanced intensity in the 390–455 nm range. This method enabled a UV dose of 60 kWh m^{-2} at 65 °C to effectively replicate approximately two years of outdoor degradation. The excellent agreement between the UV-aged and field-aged performance validates this as a practical and predictive tool for evaluating the outdoor lifetime of perovskite modules. The sub-modules demonstrated outstanding durability, with only a 2.83% decline in power conversion efficiency after three years of continuous outdoor operation. These findings support the implementation of perovskite-specific reliability testing frameworks and align with emerging international standards such as IEC TS 63624-1, highlighting the importance of tailored UV protocols in preparing perovskite technologies for commercial deployment.

Received 24th June 2025
Accepted 14th July 2025

DOI: 10.1039/d5na00622h

rsc.li/nanoscale-advances

1. Introduction

Metal halide perovskite solar cells (PSCs) have rapidly ascended as one of the most promising candidates for next-generation photovoltaic technologies, owing to their exceptional power conversion efficiencies (PCEs), cost-effective fabrication processes, and compatibility with a variety of substrates and form factors.[1,2] Since the seminal report of a 3.8% efficiency by Miyasaka and co-workers in 2009,[3] certified single-junction efficiencies have reached 27.3% as of 2025,[4] rivalling those of established crystalline silicon solar cells. These laboratory-scale achievements have progressively translated to larger-area modules; recent advances in scalable processing, such as laminar flow-assisted crystallisation, have enabled square-metre perovskite modules to surpass 18% efficiency.[5]

Despite these impressive gains in efficiency and scalability, the long-term operational stability of perovskite photovoltaic modules remains a critical barrier to commercial deployment.[6,7] Degradation mechanisms unique to perovskite materials, such as ion migration, interfacial reactions and photochemical decomposition, complicate efforts to predict module longevity under real-world conditions.[8–10] Unlike silicon-based photovoltaics, which are qualified *via* well-established certification frameworks such as IEC 61215 and IEC 61730,[11] perovskite modules currently lack dedicated protocols that reliably reflect their failure modes. Application of testing protocols originally developed for silicon photovoltaics often leads to inconsistent or misleading outcomes when evaluating perovskite stability, hindering fair cross-study comparisons and slowing progress towards industrial qualification. The International Summit on Organic Photovoltaic Stability (ISOS) introduced a suite of testing protocols tailored to emerging photovoltaic technologies, including PSCs.[12] These guidelines are valuable for harmonising research practices and promoting reproducibility; however, they are primarily intended for academic use and do not impose absolute performance thresholds or qualification criteria, which are essential for commercial adoption.

More recently, significant efforts have been devoted to refining these methodologies and understanding their implications for device physics. For instance, Zhao *et al.* conducted

[a]*Microquanta Semiconductor Co. Ltd, Hangzhou, Zhejiang 311121, China*
[b]*Three Gorges Corporation, Science and Technology Research Institute, Beijing 101199, China*
[c]*China Huadian Corporation Ltd Qinghai Company, Xining, Qinghai 810008, China*
† These authors contributed equally to this work.

high-temperature (110 °C) continuous illumination tests to quantify accelerated degradation of all-inorganic $CsPbI_3$ devices, with lifetime projections exceeding 51 000 hours at 35 °C based on Arrhenius scaling.[13] Similarly, *in situ* IV-PL coupled characterisation systems have been developed to enable real-time tracking of photodegradation pathways under damp heat conditions,[14] while light-free forward bias ageing has been proposed as a proxy for outdoor ion migration effects.[15] In parallel, high-intensity light soaking protocols (up to 4 suns) have been shown to accelerate testing throughput while preserving degradation kinetics,[16] and machine learning models trained on early-time PL absorption spectra have demonstrated predictive capability for long-term stability outcomes.[17] Moreover, recent two-year outdoor monitoring of perovskite mini-modules revealed reproducible diurnal degradation–recovery patterns, which were successfully correlated to environmental parameters using XGBoost regression.[18] These advances are complemented by consensus efforts to formalise ISOS-based stability testing specific to perovskites,[12] including strategies to mitigate iodine volatilisation and reversible photo-induced degradation under ISOS-L protocols.[19,20] Together, these studies underscore a growing sophistication in stability assessment techniques, from mechanistic studies to data-driven forecasting and consensus framework building.

Yet, the specific impact of ultraviolet light remains poorly understood, and its correlation with outdoor degradation is unclear. For example, IEC 61215 prescribes only 15 kWh m^{-2} of light exposure, far below the cumulative dose experienced in real-world operation.[11] UV and short-wavelength visible light (280–455 nm), though comprising only ~8% of AM 1.5G solar energy, are known to drive significant degradation in perovskite materials.[21,22] This spectral region affects both bulk and interfacial stability, as confirmed by our previous work and that of others.[5] Importantly, UV ageing avoids artefacts seen in outdoor tests, such as early PCE increases due to ion migration, which can obscure real degradation. Focused UV protocols offer a clearer and more reliable assessment of perovskite stability.

To address persistent gaps in the evaluation of perovskite module stability, this study presents a comprehensive three-year investigation that connects UV-induced accelerated ageing with real-world outdoor performance. In April 2021, we established a micro perovskite power station in Quzhou, Zhejiang Province, consisting of 20 sub-modules (each rated at ~13 W, totalling ~260 W), all fabricated using scalable, industry-compatible processes. These modules were installed outdoors at a fixed tilt angle and monitored continuously from 2021 to 2024 to track power output and environmental exposure. In parallel, identical modules were placed in a controlled UV ageing chamber and subjected to high-dose UVA + UVB + UVV (280–455 nm) illumination to emulate long-term photodegradation. By systematically comparing degradation trajectories under natural and accelerated conditions, we establish a quantitative correlation between UV stress and outdoor energy yield loss. This represents the first empirical mapping of its kind, offering a scientific foundation for the development of perovskite-specific ageing protocols.

2. Materials and methods

2.1. Materials

The NiO_x precursor solution was prepared by dissolving 293 g (1 mol) of $Ni(acac)_2$ $2H_2O$ (99%, Shanghai Aladdin) in 10 L of ethanol (98%, Hangzhou Orient) and 50 mL of ethanolamine. The mixture was stirred for 4 h and filtered through a 0.22 μm PTFE membrane. The solution was used within 24 h and stored in a fume hood under relative humidity below 45%. The PTAA solution was prepared by dissolving in-house synthesized poly(triaryl amine) in chlorobenzene (99%, Hangzhou Orient) at a concentration of 1.5 g L^{-1}. This solution was also filtered through a 0.22 μm PTFE membrane and renewed every 12 h under the same ambient conditions. The perovskite precursor was formulated by dissolving 553.2 g PbI_2 (98%, Zhejiang Yitai), 185.7 g FAI (98%, TCI), and 31.2 g CsI (99.9%, Zhejiang Yitai) in 1 L of DMF : DMSO (4 : 1, v/v; both 99%, Shandong Hualu-Hengsheng). After stirring for 2 h, 12.2 g MACl (15 mol%, 98%, TCI) and 10.0 g $PbCl_2$ (3 mol%, 98%, Zhejiang Yitai) were added. The final solution was filtered through a 0.22 μm PTFE membrane in a dry room (RH < 30%).[5]

2.2. Fabrication process of perovskite sub-modules

Perovskite sub-modules were fabricated on 30 cm × 40 cm × 3.2 mm FTO-coated glass substrates. Initial P1 laser scribing was performed to define isolated electrode regions. Substrates were then cleaned sequentially with detergent, deionised water, acetone, and isopropanol. All subsequent wet processes were conducted in a Class 1000 cleanroom maintained at 23–25 °C and relative humidity below 45%. The NiO_x hole transport layer was applied *via* slot-die coating and annealed in a continuous belt oven at 350 °C for 30 minutes in air. After cooling to below 30 °C, a PTAA layer was deposited using a second slot-die coater. This was followed by a brief drying step at 100 °C for 10 minutes to remove residual solvent. Once the substrate cooled to below 25 °C, the perovskite photoactive layer was deposited using a third slot-die coater. The wet film was dried in an oven and subsequently subjected to vacuum thermal annealing, resulting in a uniform and crystalline perovskite film.

Subsequent vacuum processes included thermal evaporation of 20 nm of C_{60} (Henan Fullerene Nano Material Co., Ltd, 99.9%) and 5 nm of bathocuproine, followed by deposition of 7 nm of SnO_2 *via* inline spatial ALD at 90 °C. The SnO_2 layer was grown using tetrakis(dimethylamino)tin (99.9999%) and ultrapure water (99.9999%) as precursors, supplied by Shanghai Oriphant. P2 laser scribing was carried out using a 532 nm nanosecond laser (Bellin Marble GR-40) to remove all upper layers above the FTO. The beam frequency was set to 100 kHz and the power to 5.1 W. The back electrode was deposited by magnetron sputtering: first 10 nm of ITO (In : Sn = 90 : 10) was deposited using an RF source (Hüttinger TruPlasma RF 3012), followed by 20 nm of ITO and 100 nm of Cu using a DC source (Hüttinger TruPlasma DC 3030). P3 laser scribing was then performed with a 532 nm nanosecond laser (Bellin Amber NX GR-15S) at 300 kHz and 0.8 W.

A dead zone width of 195.5 μm and pitch width of 6.3 mm were achieved, corresponding to a geometric fill factor (GFF) of 97%. P4 edge ablation was carried out with a 1064 nm nanosecond laser (Raycus RFL P1000H), using a beam frequency of 10 kHz and power of 1000 W, creating 17 mm edge clearance on all four sides. Each sub-module comprised 52 series-connected sub-cells (26 cm in length and 6.3 mm in width), with an effective area of 868.4 cm^2 (26 cm × 33.4 cm). Modules were encapsulated between two 30 cm × 40 cm × 3.2 mm tempered glass sheets using a POE encapsulant and a PIB edge sealant (Quanex, SolarGain series). In addition, a pre-cut polyolefin (Hangzhou First Applied Material, TPO series) film was gently laminated to the back, and the junction box was affixed and filled with epoxy resin, which was cured for 8 hours. Final lamination was performed at 120 °C and 90 kPa for 15 min.

2.3. Outdoor field testing and IV characterization

To establish the perovskite micro-power station, 20 perovskite sub-modules were deployed outdoors for continuous operation over a three-year period (April 2021–March 2024) in an open field in Quzhou, China. The sub-modules were mounted on a fixed rack, tilted at a 20° angle using standard aluminum brackets to optimize solar irradiance reception. All modules, each with a nominal power output of approximately 13 W, were wired in parallel and connected to a micro-inverter (Brand: Hoymiles, Model: M1-1200). Irradiance data were collected using a YIGU ML YGC-TBQ Si-pyranometer at 10-second intervals using a Picotech PT-104 datalogger. Module temperatures were monitored using TH10S-B sensors affixed to the rear of each module. Output power was tracked using Huawei SUN2000-125KTL-JPH0 maximum power point (MPP) trackers. Daily electricity generation was monitored, and monthly and annual performance ratios (PR) as well as Equivalent Full Sun Hours (EFSH) were calculated to assess the system's operational stability and solar resource availability. Periodic removal of the modules allowed for performance measurements under Standard Test Conditions (STC) with 1 Sun irradiation.

Indoor IV measurements were performed using a 2 m × 1.5 m Class AAA steady-state solar simulator (LASS200150, Eternal Sun). The voltage scan was set from 0 to 60 V with a step size of 150 mV, resulting in a total of 400 data points. The scan duration was 30 s. Before any stress testing or outdoor exposure, the initial power conversion efficiency (PCE) of each mini-module was recorded under standard conditions.

2.4. Spectral-enhanced UV-blue-violet accelerated ageing and damp-heat stability evaluation

To evaluate photostability under accelerated conditions, perovskite sub-modules from the same production batch as those deployed in the field were subjected to ultraviolet (UV) ageing using a GRO-SUV3226T chamber (Shanghai Reichy), which offers a large exposure area of 3200 mm × 2600 mm. The chamber operated at a controlled temperature of 60 °C ± 5 °C, with combined UVA and UVB irradiance maintained at 200 ± 30 W m^{-2} and a UVA : UVB ratio of 5–9%, consistent with IEC 61215 specifications. Irradiance was continuously monitored at the module plane using an *in situ* sensor, and the cumulative UV dose was obtained by integrating spectral power over the test duration.

To accurately characterise the spectral power distribution (SPD) during UV ageing, real-time spectral measurements were carried out using a fibre-optic spectrometer manufactured by Avasolar (Model AVA-UVX300). The system incorporates a calibrated spectrometer, a cosine-corrected diffuser, and a photodiode array, enabling continuous measurements across the 200–800 nm range with a spectral resolution of 1 nm, wavelength accuracy of ±1.0 nm, and intensity resolution better than 5%. During operation, the sensor head was positioned at the same height and angle as the module test surface to ensure that the recorded spectra faithfully represented the actual irradiance received by the samples within the UV ageing chamber. By integrating spectral irradiance across the UVA (320–390 nm), UVB (280–320 nm), and violet-blue UVV (390–455 nm) regions, the relative contributions of each spectral band to device degradation were quantitatively assessed. This characterisation provided essential spectral input parameters for establishing a direct correlation between the ageing spectrum and the performance degradation observed in perovskite modules.

In parallel, damp-heat (DH) ageing tests were conducted to assess the moisture and thermal robustness of the module architecture. Modules were placed in a climate chamber at 85 °C and 85% relative humidity, in line with IEC 61215 DH protocols. This test focused on identifying encapsulation-related failure modes such as delamination, corrosion, and ion migration, complementing the UV and field ageing studies by providing a broader view of environmental reliability.

3. Results and discussion

3.1. Configuration and structural design of the perovskite micro power station

A perovskite micro photovoltaic (PV) power station was constructed in April 2021 in Quzhou, Zhejiang Province, China, a region characterised by a humid subtropical climate. The station comprises 20 perovskite sub-modules, each with a geometrical size of 300 mm × 400 mm and a nominal output power of approximately 13 W, resulting in a total installed capacity of ~260 W. All sub-modules were electrically connected in parallel and routed through a micro-inverter, which interfaces with the AC grid. To optimise incident solar irradiance, the modules were mounted at a fixed tilt angle of 20°, using standard anodised aluminium alloy frames.

Fig. 1a illustrates the outdoor deployment of the micro power station. Fig. 1b shows the parallel wiring diagram of the 20 modules, while Fig. 1c presents the distribution of their rated power outputs. As detailed in Table 1, the average power conversion efficiency (PCE) across all 20 modules at the beginning of deployment was 15.94%. The sub-modules employed in this study follow a typical inverted (p–i–n) structure, comprising a NiOx hole transport layer, a PTAA interfacial layer, an $FA_{0.9}Cs_{0.1}PbI_3$ perovskite light-absorbing layer, a fullerene-based C_{60} electron transport layer, an SnO_2 interlayer, and an ITO buffer, capped with a Cu metal electrode.[23,24] The encapsulation

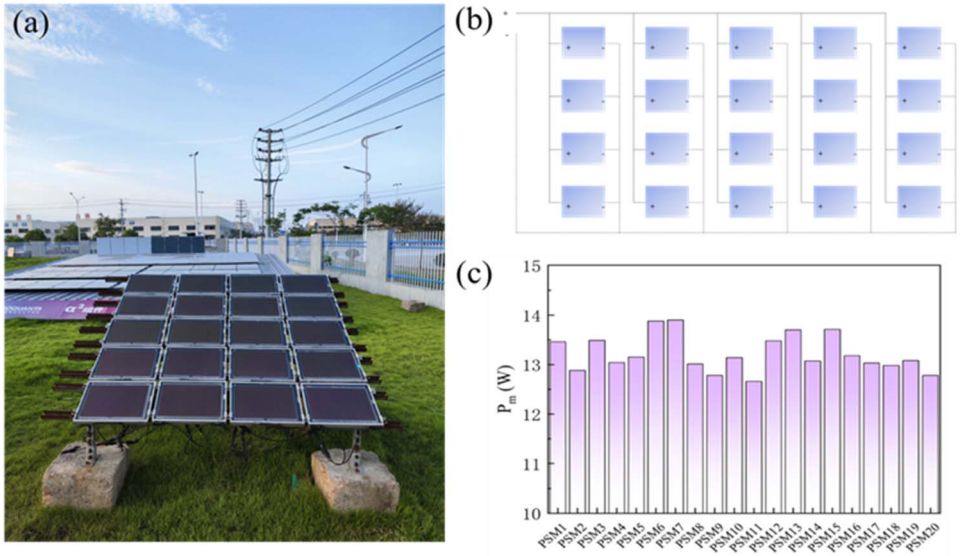

Fig. 1 (a) Outdoor view of the perovskite micro power station deployed in Quzhou. (b) Connection diagram showing parallel wiring of 20 perovskite sub-modules. (c) Histogram of rated maximum power (P_{max}) for the 20 modules.

utilised a POE (polyolefin elastomer) film, PIB (polyisobutylene) edge sealant, and dual-side tempered glass for moisture and oxygen barrier protection. The internal structural configuration is shown schematically in Fig. 2, designed to facilitate charge extraction, minimise recombination losses, and enhance environmental stability—factors critical for maintaining long-term outdoor operability.

3.2. Performance of the perovskite micro power station over three years of outdoor operation

To comprehensively assess the long-term performance of the perovskite-based micro power station under real-world environmental conditions, a continuous three-year outdoor monitoring campaign was conducted. This investigation was designed to capture not only the seasonal and interannual variations in energy output but also the operational resilience and intrinsic material stability of the deployed $FA_{0.9}Cs_{0.1}PbI_3$-based modules. The monitoring strategy integrated system-level energy output metrics with module-level degradation assessments, offering a holistic picture of photovoltaic performance in subtropical climates.

Throughout the monitoring period, a suite of environmental and operational parameters was systematically recorded. These included solar irradiance, ambient and module temperatures, real-time output power, daily energy generation, and critical performance indicators such as equivalent full sun hours (EFSH) and performance ratio (PR).[5] These parameters collectively enabled detailed analysis of both solar resource availability and photovoltaic system conversion efficiency, accounting for dynamic weather patterns and seasonal solar flux variations.

Fig. 3 illustrates the monthly evolution of EFSH over the three-year period in Quzhou, where the micro power station was installed. The EFSH was computed using irradiance data collected at 10-second intervals by calibrated pyranometers and normalised to the standard test condition (STC) irradiance of 1000 W m^{-2}. This metric provides a time-integrated representation of solar input, reflecting the cumulative hours during which the system effectively received "1 Sun" of irradiance:

$$\mathrm{EFSH(h)} = \frac{\text{total energy yielded (kWh)}}{\text{rated power output at STC (kWp)}} \quad (1)$$

This formulation allows EFSH to function as a temporally standardised solar availability metric, independent of daily fluctuations in light intensity. Notably, the highest EFSH values were consistently recorded in July and August of each year, corresponding to periods of extended daylight and high solar insolation. Seasonal variability was evident, with expected declines during winter months; however, comparison across the same months in different years revealed minimal interannual variation, indicating stable and consistent system performance. A pronounced increase in EFSH was observed in July and August 2022, which correlated well with independently measured

Table 1 Specific performance parameters of the 20 perovskite sub-modules used in the micro power station

Parameter	V_{oc}/V	I_{sc}/mA	P_{max}/W	J_{sc}/mA cm^{-2}	FF	PCE/%
Average value	53.98	0.37	13.32	22.62	0.67	15.94
Standard deviation	1.66	0.00	0.43	0.13	0.02	0.52

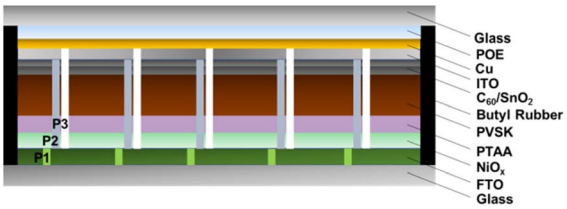

Fig. 2 Cross-sectional schematic of the perovskite sub-module, showing all functional layers and encapsulation configuration.

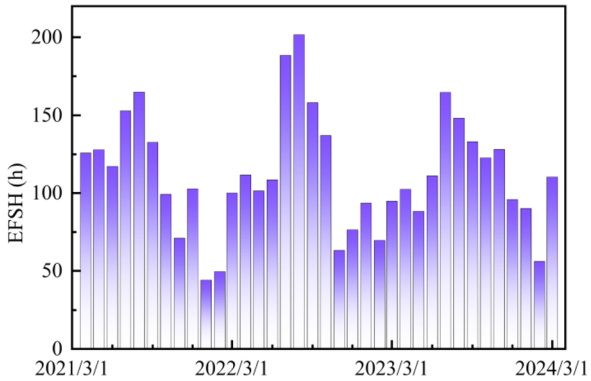

Fig. 3 Monthly EFSH for the perovskite modules over three operational years in Quzhou.

increases in solar irradiance, reinforcing the sensitivity and reliability of the EFSH metric.

To complement these monthly summaries, Fig. 4 presents high-resolution time-series data of both daily irradiance (bottom) and corresponding energy yield (top) over the full operational period. The data demonstrate a strong correlation between incident solar energy and system output, underscoring the robust light-harvesting performance of the perovskite modules. Remarkably, even during extended periods of overcast weather or diffuse light conditions, the system maintained a relatively stable output. This consistent performance highlights a notable advantage of the $FA_{0.9}Cs_{0.1}PbI_3$ composition, its superior low-light response, which makes it particularly suitable for deployment in regions characterised by high humidity or frequent cloud cover.

To quantitatively evaluate the system's real-world efficiency, we further analysed the performance ratio (PR), which serves as a normalised indicator of operational efficiency by comparing actual energy output to theoretical yield under STC. In eqn (2), PR is calculated as the quotient of the specific yield factor (Y_f) and the reference yield (Y_r):[25–28]

$$\mathrm{PR} = \frac{Y_f}{Y_r} = \frac{\int_{t_1}^{t_2} P_{\mathrm{mpp\_actual}}(t)\mathrm{d}t}{P_{\mathrm{psm}} \times \int_{t_1}^{t_2} \mathrm{irradiance}(t)\mathrm{d}t} \quad (2)$$

Here, P_{mpp} actual is the measured power output of the PV system from the AC side of the microinverter. P_{psm} is the power output of the PV system under the condition of standard solar irradiance (1000 W m^{-2}). Irradiance presents the value of real-time irradiance, which was collected every 10 s. $t1$ and $t2$ represent the testing times. As shown in Fig. 5, the monthly PR values over three years exhibited remarkable consistency, with only a marginal decline observed, from 102.1% in the first operational year to 101.3% in the third year, amounting to a total degradation of just 0.78%. The calculated PR values were averaged from daily measurements, and the resulting annual values are summarised in Table 2.

These findings reinforce the excellent operational reliability and long-term energy conversion efficiency of the system. Despite exposure to natural weathering effects, temperature cycling, and environmental stressors, the PR decline remained negligible, reflecting the robustness of both the device architecture and the system-level design.[29]

In addition to energy output metrics, we performed laboratory-based evaluations to assess the intrinsic material stability of the perovskite modules. Each year, the 20 perovskite sub-modules were disassembled and tested under standard test conditions (1000 W m^{-2}, 25 °C AM 1.5G). As shown in Fig. 6, the power conversion efficiency (PCE) degradation rates were determined to be 1.6% in the first year, followed by only 0.7% in both the second and third years. These results confirm that the perovskite sub-modules maintained excellent material and operational stability over the full three-year outdoor deployment period.

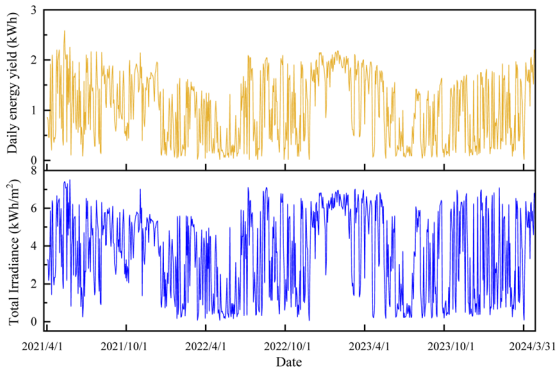

Fig. 4 Daily energy yield (top) and corresponding solar irradiance (bottom) over a three-year period.

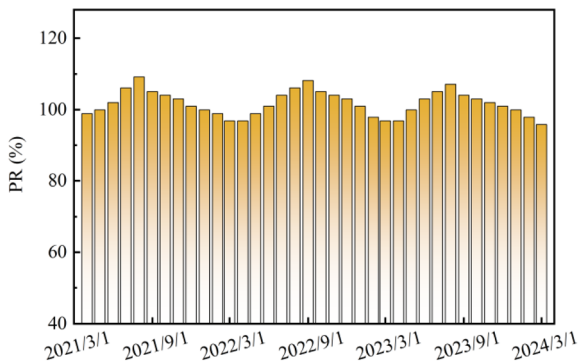

Fig. 5 Monthly performance ratio (PR) values of the perovskite micro power station over a three-year period.

Table 2 Annual average PR values of the perovskite micro power station over three years of outdoor operation

Period	Annual average PR (%)
2021-04 to 2022-03	102.10
2022-04 to 2023-03	101.90
2023-04 to 2024-03	101.30

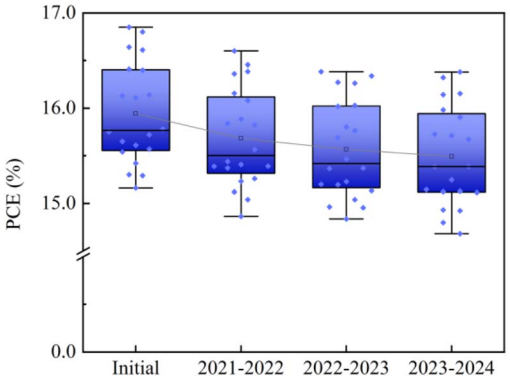

Fig. 6 Annual degradation of power conversion efficiency (PCE) of perovskite sub-modules over three years of outdoor operation.

3.3. UV-blue-violet spectral ageing as a predictive tool for outdoor lifetime of perovskite modules

Evaluating the long-term outdoor stability of perovskite solar modules (PSMs) through real-time field testing is inherently time-consuming. To address this limitation and establish a predictive ageing methodology, we adopted an accelerated ultraviolet (UV) ageing protocol based on the spectral characteristics of natural sunlight.

Numerous studies have demonstrated that UV photons in sunlight, particularly within the UVA (320–390 nm) and UVB (280–320 nm) regions, are critical contributors to the photo-induced degradation of perovskite materials.[30,31] The standard AM 1.5G solar spectrum contains approximately 38.8 W m^{-2} in this UV range, which accounts for about 4.5% of the total irradiance (see Table 3). Based on this, and given that the effective full sun hours (EFSH) in Quzhou average around 1200–1600 h per year, the corresponding annual UV dose is estimated at approximately 47–60 kWh m^{-2}. In regions with higher solar irradiance, where EFSH can reach 1900 h per year, the annual UV dose increases to about 74 kWh m^{-2} (Fig. 7).

To simulate two years of UV exposure under field conditions, we exposed the modules to a UV dose of 60 kWh m^{-2} across the

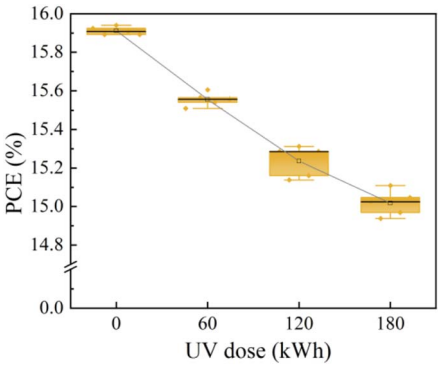

Fig. 7 PCE degradation after 60, 120, and 180 kWh m^{-2} UV doses.

280–455 nm spectral range at 65 °C for 14 days. This range includes not only UVA and UVB, but also the blue-violet region (390–455 nm), where the spectral intensity of the artificial light source is approximately four times greater than that of the AM 1.5G spectrum (see Fig. S4). The inclusion of this high-energy region is especially relevant, as it accelerates degradation through mechanisms such as trap-state formation and ion migration. After the accelerated ageing test, the modules retained 96.86% of their initial PCE, corresponding to a degradation of only 3.14%. Although this value is slightly higher than the degradation observed after one year of field exposure (1.6%), it is justifiable given the increased UV dose and elevated testing temperature. The use of a condensed timescale and intensified spectral power further supports the effectiveness of this accelerated protocol.

To ensure that the degradation observed was primarily due to light-induced mechanisms rather than packaging failure, a separate damp-heat (DH) test was performed on the same module design for 3000 hours at 85 °C and 85% relative humidity. The results, shown in Fig. 8, confirmed minimal PCE decline, indicating that the encapsulation was effective in preventing moisture ingress. This reinforces the conclusion that the performance degradation observed in both UV and outdoor ageing tests stems from intrinsic material and photo-physical processes rather than environmental ingress.

Extended testing with a UV dose of 180 kWh m^{-2} resulted in a PCE loss of approximately 7.3%, which is more than twice the degradation observed over three years of natural ageing.[32–38] These results indicate that a UV dose of 60 kWh m^{-2} approximates two years of outdoor exposure in subtropical climates such as Quzhou. Assuming a linear degradation trend, the estimated $T90$ (time to reach 90% of initial PCE) for $FA_{0.9}Cs_{0.1}PbI_3$-based modules is around nine years.

Table 3 Irradiance contributions (W m^{-2}) across spectral regions for representative light sources

	Irradiance @ certain range, W m^{-2}			
Light source	UVA (320–390)nm	UVB (280–320)nm	UVC (250–260)nm	UVV (390–455)nm
AM 1.5G	3.73	0.15		7.78
UV aging chamber	21.11	1.32	—	39.91

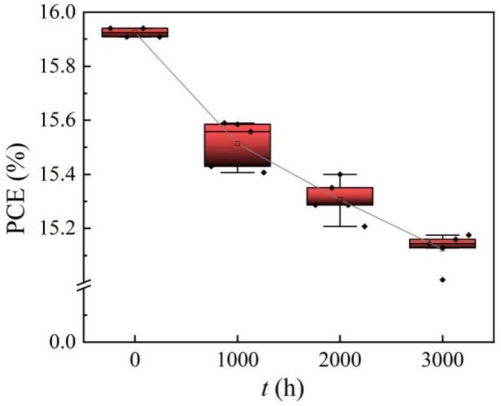

Fig. 8 Damp-heat accelerated ageing data for perovskite modules.

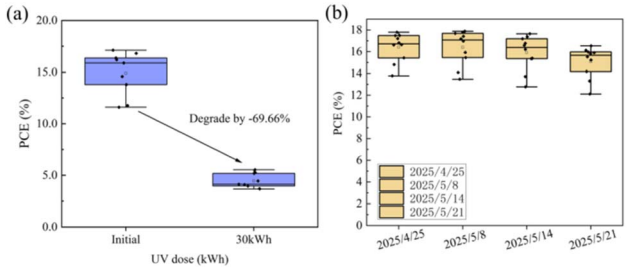

Fig. 9 (A) PCE degradation of $MAPbI_3$ perovskite sub-modules under UV accelerated ageing with a total dose of 30 kWh m^{-2}. (B) PCE change of the same modules after 25 days of outdoor exposure.

Nonetheless, we acknowledge that such a direct correlation may not be universally applicable across all perovskite systems. To highlight the composition-dependent nature of UV degradation,[39–41] we conducted a comparative test using $MAPbI_3$-based modules under identical UV conditions. After receiving just 30 kWh m^{-2} of UV exposure, the PCE of $MAPbI_3$ modules dropped precipitously by 69.66%, indicating extremely poor UV resilience. In contrast, the same $MAPbI_3$ devices, when deployed outdoors at moderate temperatures (~40 °C, ~70 peak sun hours), retained 98% of their initial efficiency after 27 days. Even in a hotter scenario (device temperature ~60 °C), the degradation only increased modestly to 94%, as reported by Huang *et al.*[42] These contrasting behaviours emphasise the importance of spectral weighting and material sensitivity in ageing studies. The $FA_{0.9}Cs_{0.1}PbI_3$ composition used in our study thus offers a far superior stability profile under both UV-rich and natural conditions. As demonstrated in our supplementary test with the less stable $MAPbI_3$ composition, a 20 kWh UV dose caused a 68.8% PCE loss, while the same device retained ~98% of efficiency after 27 days of real-world exposure. This stark contrast highlights how overestimating UV sensitivity can lead to underestimating actual outdoor lifetime, emphasising that composition-specific calibrations are essential. Therefore, although the $FA_{0.9}Cs_{0.1}PbI_3$ system represents a widely adopted, well-stabilised benchmark, its ageing kinetics should not be generalized. The predictive accuracy of UV-based ageing must be validated or re-parameterized when applied to new perovskite formulations or different climate conditions. Yet, the strong correlation between UV ageing rate and outdoor degradation directionality still holds, providing critical insight into dominant degradation pathways such as ion migration and trap-state formation.

Our results suggest that UV ageing tests, when carefully calibrated for dose, spectrum, and temperature, can serve as reliable proxies for long-term outdoor performance. The clean and linear degradation observed under UV exposure avoids the confounding effects of environmental variability and burn-in, offering higher resolution for kinetic modelling.

This approach echoes trends in the crystalline silicon industry, where UV doses of 240 kWh m^{-2} are standardised for long-term qualification.[43] Recently, a draft IEC technical specification (IEC TS 63624-1 ED1), led by Canadian Solar, proposed a dose of 120 kWh m^{-2} to represent 5–8 years of real-world UV exposure. These converging insights suggest that spectrum-weighted, dose-controlled UV protocols should be considered a central component of accelerated reliability testing for perovskite PV technologies. In particular, the inclusion of high-intensity UVV wavelengths may offer diagnostic value in uncovering degradation mechanisms relevant to advanced multi-cation perovskite formulations (Fig. 9).

In summary, our findings confirm that UV-blue-violet ageing is not only reflective of real-world degradation pathways but also offers a flexible tool for lifetime prediction, provided the correlation is tailored to the material system in question. Further work is needed to expand this methodology across the evolving landscape of perovskite materials.

4. Conclusion

In this work, we present a comprehensive three-year field evaluation of a perovskite-based micro photovoltaic power station, comprising 20 perovskite sub-modules deployed in the subtropical climate of Quzhou, China. Each module was fabricated with an inverted (p–i–n) architecture and encapsulated using industrially scalable materials and methods. The system was monitored in real time for energy output, environmental conditions, and performance metrics, including equivalent full sun hours (EFSH) and performance ratio (PR).

Our results demonstrate the excellent long-term operational stability of the perovskite modules under real-world conditions. After three years of continuous outdoor deployment, the system exhibited only a 2.83% reduction in average power conversion efficiency (PCE), and a marginal 2.47% decline in annual PR. These findings establish one of the longest and most complete real-time outdoor performance datasets for scalable perovskite solar modules to date, reinforcing the field durability of halide perovskite photovoltaics.

To further probe degradation pathways, we conducted controlled UV ageing tests, applying cumulative doses of 60 and 180 kWh m^{-2} at 65 °C under a spectrum-enhanced chamber. The results revealed a quantitative correlation between UV-induced degradation and natural outdoor ageing, suggesting that spectrum-weighted, dose-controlled UV protocols can be

reliably used to predict field performance, provided that the spectral match and temperature settings are appropriately tuned.

A critical innovation of this study lies in the establishment of a dose equivalence framework, whereby 60 kWh m^{-2} of UV exposure is shown to approximate two years of outdoor ageing in a subtropical setting. This mapping enables accelerated stability assessments of new perovskite formulations without the need for multi-year field campaigns. Furthermore, comparative studies with $MAPbI_3$ modules underscore the importance of compositional engineering for enhancing photostability and spectral resilience.

Our findings also align with, and help substantiate, emerging international standards. Specifically, the degradation kinetics observed in our UV chamber testing parallel those proposed in the IEC TS 63624-1 ED1 technical draft, which recommends 120 kWh m^{-2} of UV exposure to represent 5–8 years of real-world use. This convergence of academic and industrial methodologies strengthens the case for integrating UV stress testing into the standard qualification pipeline for perovskite photovoltaics.

In summary, this study not only provides critical field data on the long-term stability of scalable perovskite modules but also introduces a validated UV acceleration methodology, bridging the gap between laboratory simulation and real-world operation. By combining systematic outdoor monitoring with accelerated spectral ageing, we offer a practical and predictive framework for reliability assessment, one that could facilitate the commercial deployment of perovskite technologies at a meaningful scale.

Conflicts of interest

The authors declare no conflicts of interest in relation to the work presented here.

Data availability

Data are available on request from the authors.

Further details of module performance and related characterisation data are provided in the SI. See DOI: **https://doi.org/10.1039/d5na00622h**.

Acknowledgements

This research was funded by the Scientific Research Project of China Three Gorges Corporation (Grant No. 202303014). The authors gratefully acknowledge the support of the Scientific Research Project of China Three Gorges Corporation (Project No. 202303014), which has significantly advanced research in perovskite photovoltaic technology and enabled key experimental investigations. We also express our sincere gratitude to the Scientific Research Project of China Three Gorges Corporation (Project No. 202103483) for its contribution to the development of perovskite photovoltaic technologies. Furthermore, we are thankful for the support of the Key R&D Programme of Zhejiang (Project No. 2022C01104) and the Key R&D Programme of Quzhou (Project No. 2021Z05), both of which have fostered innovation in high-efficiency perovskite photovoltaic applications and renewable energy technologies.

References

1 M. A. Green, A. Ho-Baillie and H. J. Snaith, *Nat. Photonics*, 2014, **8**, 506–514.
2 A. Miyata, A. Mitioglu, P. Plochocka, O. Portugall, J. T.-W. Wang, S. D. Stranks, H. J. Snaith and R. J. Nicholas, *Nat. Phys.*, 2015, **11**, 582–587.
3 A. Kojima, K. Teshima, Y. Shirai and T. Miyasaka, *J. Am. Chem. Soc.*, 2009, **131**, 6050–6051.
4 M. A. Green, E. D. Dunlop, M. Yoshita, N. Kopidakis, K. Bothe, G. Siefer, X. Hao and J. Y. Jiang, *Prog. Photovoltaics Res. Appl.*, 2025, **33**, 795–810.
5 B. Yan, W. Dai, Z. Wang, Z. Zhong, L. Zhang, M. Yu, Q. Zhou, Q. Ma, K. Yan, L. Zhang, Y. Yang and J. Yao, *Science*, 2025, **388**, 5001.
6 M. Othman, Q. Jeangros, M. U. Rothmann, Y. Jiang, C. Ballif, A. Hessler-Wyser and C. M. Wolff, *Adv. Mater.*, 2025, **37**, 2409742.
7 X. Luo, X. Lin, F. Gao, Y. Zhao, X. Li, L. Zhan, Z. Qiu, J. Wang, C. Chen, L. Meng, X. Gao, Y. Zhang, Z. Huang, R. Fan, H. Liu, Y. Chen, X. Ren, J. Tang, C.-H. Chen, D. Yang, Y. Tu, X. Liu, D. Liu, Q. Zhao, J. You, J. Fang, Y. Wu, H. Han, X. Zhang, D. Zhao, F. Huang, H. Zhou, Y. Yuan, Q. Chen, Z. Wang, S. F. Liu, R. Zhu, J. Nakazaki, Y. Li and L. Han, *Sci. China Chem.*, 2022, **65**, 2369–2416.
8 P. Tolueinia, H. Khassaf, A. Shirazi Amin, Z. M. Tobin, S. P. Alpay and S. L. Suib, *ACS Appl. Energy Mater.*, 2020, **3**, 8240–8248.
9 D. B. Khadka, Y. Shirai, M. Yanagida and K. Miyano, *ACS Appl. Energy Mater.*, 2021, **4**, 11121–11132.
10 Z. Peng, A. Vincze, F. Streller, V. M. Le Corre, K. Zhang, C. Li, J. Tian, C. Liu, J. Luo, Y. Zhao, A. Späth, R. Fink, T. Heumüller, A. Osvet, N. Li, M. Stolterfoht, L. Lüer and C. J. Brabec, *Energy Environ. Sci.*, 2024, **17**, 8313–8324.
11 IEC 61215:2021, *Terrestrial Photovoltaic (PV) Modules-Design Qualification and Type Approval*, International Electrotechnical Commission, Geneva, 2021.
12 M. V. Khenkin, E. A. Katz, A. Abate, G. Bardizza, J. J. Berry, C. Brabec, F. Brunetti, V. Bulović, Q. Burlingame, A. Di Carlo, R. Cheacharoen, Y.-B. Cheng, A. Colsmann, S. Cros, K. Domanski, M. Dusza, C. J. Fell, S. R. Forrest, Y. Galagan, D. Di Girolamo, M. Grätzel, A. Hagfeldt, E. von Hauff, H. Hoppe, J. Kettle, H. Köbler, M. S. Leite, S. Liu, Y.-L. Loo, J. M. Luther, C.-Q. Ma, M. Madsen, M. Manceau, M. Matheron, M. McGehee, R. Meitzner, M. K. Nazeeruddin, A. F. Nogueira, Ç. Odabaşı, A. Osherov, N.-G. Park, M. O. Reese, F. De Rossi, M. Saliba, U. S. Schubert, H. J. Snaith, S. D. Stranks, W. Tress, P. A. Troshin, V. Turkovic, S. Veenstra, I. Visoly-Fisher, A. Walsh, T. Watson, H. Xie, R. Yıldırım, S. M. Zakeeruddin, K. Zhu and M. Lira-Cantu, *Nat. Energy*, 2020, **5**, 35–49.

13 C. Fei, A. Kuvayskaya, X. Shi, M. Wang, Z. Shi, H. Jiao, T. J. Silverman, M. Owen-Bellini, Y. Dong, Y. Xian, R. Scheidt, X. Wang, G. Yang, H. Gu, N. Li, C. J. Dolan, Z. J. D. Deng, D. N. Cakan, D. P. Fenning, Y. Yan, M. C. Beard, L. T. Schelhas, A. Sellinger and J. Huang, *Science*, 2024, **384**, 1126–1134.
14 A. Levtchenko, A. Julien, D. McDermott, J.-B. Puel, J.-F. Guillemoles, D. Ory and D. Suchet, *Sol. RRL*, 2024, **8**, 2400511.
15 U. Erdil, M. Khenkin, M. Remec, Q. Emery, V. Sudhakar, R. Schlatmann, A. Abate, E. A. Katz and C. Ulbrich, *ACS Energy Lett.*, 2025, **10**, 1529–1537.
16 F. Ren, Q. Lu, X. Meng, J. Zhou, R. Chen, J. Wang, H. Wang, S. Liu, Z. Liu and W. Chen, *J. Energy Chem.*, 2024, **94**, 1–9.
17 Z. Liu, J. Zhang, G. Rao, Z. Peng, Y. Huang, S. Arnold, B. Liu, C. Deng, C. Li, H. Li, H. Zhi, Z. Zhang, W. Zhou, J. Hauch, C. Yan, C. J. Brabec and Y. Zhao, *ACS Energy Lett.*, 2024, **9**, 662–670.
18 V. Paraskeva, M. Norton, A. Livera, A. Kyprianou, M. Hadjipanayi, E. Peraticos, A. Aguirre, S. Ramesh, T. Merckx, R. Ebner, T. Aernouts, A. Krishna and G. E. Georghiou, *ACS Energy Lett.*, 2024, **9**, 5081–5091.
19 X. Li, H. Yang, A. Liu, C. Lu, H. Yuan, W. Zhang and J. Fang, *Energy Environ. Sci.*, 2023, **16**, 6071–6077.
20 X. Lu, K. Sun, Y. Wang, C. Liu, Y. Meng, X. Lang, C. Xiao, R. Tian, Z. Song, Z. Zhu, M. Yang, Y. Bai and Z. Ge, *Adv. Mater.*, 2024, **36**, 2400852.
21 W. Wang, J. Zhang, K. Lin, J. Wang, X. Zhang, B. Hu, Y. Dong, D. Xia and Y. Yang, *Adv. Mater.*, 2023, **35**, 2306140.
22 M. Tao, Y. Wang, K. Zhang, Z. Song, Y. Lan, H. Guo, L. Guo, X. Zhang, J. Wei, D. Cao and Y. Song, *Joule*, 2024, **8**, 3142–3152.
23 X. Lian, J. Chen, S. Shan, G. Wu and H. Chen, *ACS Appl. Mater. Interfaces*, 2020, **12**, 46340–46347.
24 M. Wong-Stringer, O. S. Game, J. A. Smith, T. J. Routledge, B. A. Alqurashy, B. G. Freestone, A. J. Parnell, N. Vaenas, V. Kumar, M. O. A. Alawad, A. Iraqi, C. Rodenburg and D. G. Lidzey, *Adv. Energy Mater.*, 2018, **8**, 1801234.
25 A. Ziane, A. Necaibia, N. Sahouane, R. Dabou, M. Mostefaoui, A. Bouraiou, S. Khelifi, A. Rouabhia and M. Blal, *Sol. Energy*, 2021, **220**, 745–757.
26 D. Hassan Daher, L. Gaillard and C. Ménézo, *Renew. Energy*, 2022, **187**, 44–55.
27 R. Ihaddadene, M. El hassen Jed, N. Ihaddadene and A. De Souza, *Sol. Energy*, 2022, **232**, 52–62.
28 A. Limmanee, S. Songtrai, N. Udomdachanut, S. Kaewniyompanit, Y. Sato, M. Nakaishi, S. Kittisontirak, K. Sriprapha and Y. Sakamoto, *Renew. Energy*, 2017, **102**, 199–204.
29 K. Kunaifi, A. Reinders, S. Lindig, M. Jaeger and D. Moser, *Appl. Sci.*, 2020, **10**, 5412.
30 J. Villa and A. Martí, *IEEE J. Photovoltaics*, 2017, **7**, 1479–1484.
31 J. Sherozbek, J. Park, M. S. Akhtar and O. B. Yang, *Energies*, 2023, **16**, 1353.
32 Q. Li, Y. Zheng, H. Wang, X. Liu, M. Lin, X. Sui, X. Leng, D. Liu, Z. Wei, M. Song, D. Li, H. G. Yang, S. Yang and Y. Hou, *Science*, 2025, **387**, 1069–1077.
33 L. Shi, M. P. Bucknall, T. L. Young, M. Zhang, L. Hu, J. Bing, D. S. Lee, J. Kim, T. Wu, N. Takamure, D. R. McKenzie, S. Huang, M. A. Green and A. W. Y. Ho-Baillie, *Science*, 2020, **368**, 2412.
34 C. Liu, M. Cai, Y. Yang, Z. Arain, Y. Ding, X. Shi, P. Shi, S. Ma, T. Hayat, A. Alsaedi, J. Wu, S. Dai and G. Cao, *J. Mater. Chem. A*, 2019, **7**, 11086–11094.
35 J. H. Heo, Y. K. Choi, C. W. Koh, H. Y. Woo and S. H. Im, *Adv. Mater. Technol.*, 2019, **4**, 1800390.
36 R. Gehlhaar, T. Merckx, W. Qiu and T. Aernouts, *Glob. Chall.*, 2018, **2**, 1800008.
37 S. Zhang, T. Xu, P. Wu, J. Pan, W. Zhang and W. Song, *J. Mater. Chem. C*, 2024, **12**, 4676–4681.
38 Z. Liang, Y. Zhang, H. Xu, W. Chen, B. Liu, J. Zhang, H. Zhang, Z. Wang, D.-H. Kang, J. Zeng, X. Gao, Q. Wang, H. Hu, H. Zhou, X. Cai, X. Tian, P. Reiss, B. Xu, T. Kirchartz, Z. Xiao, S. Dai, N.-G. Park, J. Ye and X. Pan, *Nature*, 2023, **624**, 557–563.
39 S.-W. Lee, S. Kim, S. Bae, K. Cho, T. Chung, L. E. Mundt, S. Lee, S. Park, H. Park, M. C. Schubert, S. W. Glunz, Y. Ko, Y. Jun, Y. Kang, H.-S. Lee and D. Kim, *Sci. Rep.*, 2016, **6**, 38150.
40 R. Liu, L. Wang, Y. Fan, Z. Li and S. Pang, *RSC Adv.*, 2020, **10**, 11551–11556.
41 Z. Qin, J. A. Caraveo-Frescas, L. Fernandez-Izquierdo, M. J. Arellano-Jimenez, F. S. Aguirre-Tostado, M. G. Reyes-Banda and M. A. Quevedo-Lopez, *ACS Omega*, 2024, **9**, 26683–26691.
42 B. Chen, J. Song, X. Dai, Y. Liu, P. N. Rudd, X. Hong and J. Huang, *Adv. Mater.*, 2019, **31**, 1902413.
43 F. T. Thome, P. Meßmer, S. Mack, E. Schnabel, F. Schindler, W. Kwapil and M. C. Schubert, *Sol. RRL*, 2024, **8**, 2400628.